

This is the accepted manuscript made available via CHORUS. The article has been published as:

Pressure-induced metallization in the absence of a structural transition in the layered ferromagnetic insulator  $\text{Cr}_2\text{Ge}_2\text{Te}_6$

Weizhao Cai, Luo Yan, Su Kong Chong, Jingui Xu, Dongzhou Zhang, Vikram V. Deshpande, Liujiang Zhou, and Shanti Deemyad

Phys. Rev. B **106**, 085116 — Published 9 August 2022

DOI: [10.1103/PhysRevB.106.085116](https://doi.org/10.1103/PhysRevB.106.085116)

# **Pressure-induced metallization with absence of structural transition in layered ferromagnetic insulator $\text{Cr}_2\text{Ge}_2\text{Te}_6$**

Weizhao Cai<sup>1,2,\*</sup>, Luo Yan<sup>3</sup>, Su Kong Chong<sup>2</sup>, Jingui Xu<sup>4</sup>, Dongzhou Zhang<sup>4</sup>, Vikram V Deshpande<sup>2</sup>, Liujiang Zhou<sup>3,\*</sup>, Shanti Deemyad<sup>2,\*</sup>

<sup>1</sup> *School of Materials and Energy, University of Electronic Science and Technology of China, Chengdu 611731, Sichuan, China*

<sup>2</sup> *Department of Physics and Astronomy, University of Utah, Salt Lake City, Utah 84112, United States*

<sup>3</sup> *School of Physics, University of Electronic Science and Technology of China, Chengdu 611731, Sichuan, China*

<sup>4</sup> *PX2, Hawaii Institute of Geophysics and Planetology, University of Hawaii at Manoa, Honolulu, Hawaii 96822, United States*

Corresponding authors:

W. C.: wzcai@uestc.edu.cn

L. Z.: ljzhou86@uestc.edu.cn

S. D.: Deemyad@physics.utah.edu

**ABSTRACT:** We report the crystallographic and electrical transport properties of single crystals of ferromagnetic two-dimensional (2-D) material  $\text{Cr}_2\text{Ge}_2\text{Te}_6$  under high pressure. In contrast to previous studies, our high-pressure single crystal X-ray diffraction under hydrostatic conditions shows prominent anisotropic compressibility in the layered structure of the crystalline  $R\bar{3}$  phase of  $\text{Cr}_2\text{Ge}_2\text{Te}_6$  without any structural phase transitions up to 20 GPa. Our data confirm a distinct and irreversible crystalline-amorphous transformation in  $\text{Cr}_2\text{Ge}_2\text{Te}_6$ . The loss of crystallinity starts at 20 GPa, however, the crystalline phase and amorphous state coexist even at the maximum pressure of 31.2 GPa. High pressure powder X-ray diffraction data and electrical resistivity measurements of  $\text{Cr}_2\text{Ge}_2\text{Te}_6$  using NaCl as pressure transmitting medium reveal an insulator to metal transition in the absence of a phase transition at  $\sim 3.9$  GPa; at a considerably lower pressure than the previously reported (7-14 GPa). DFT calculations demonstrate the density of states around the Fermi level are primarily dominated by Cr-3*d* and Te-5*p* states. Hence the large reduction of Cr-Te bond lengths within the  $\text{CrTe}_6$  octahedra under compression is most likely responsible for the band gap closure. This study clarifies the phase stability and onset of metallization pressure in the  $\text{Cr}_2\text{Ge}_2\text{Te}_6$  sample are sensitive to the hydrostatic environments and demonstrates how pressure can be used to tune the physical properties of 2-D ferromagnetic compounds.

## I. INTRODUCTION

The discovery of magnetism in two-dimensional (2-D) materials with layers interlinked through van der Waals (vdW) interactions has attracted intense interest due to their potential applications in new spintronics, multiferroics and even possibility of discovering new physics such as Kitaev quantum spin liquid states [1,2]. Ferromagnetic insulators such as chromium trihalides  $\text{CrX}_3$  ( $\text{X} = \text{Br}$  and  $\text{I}$ ) and ternary chromium-based tritellurides  $\text{Cr}_2\text{Z}_2\text{Te}_6$  ( $\text{Z} = \text{Si}$  and  $\text{Ge}$ ) are few typical vdW materials demonstrate ferromagnetic order from bulk crystals to monolayer limit [3,4]. In the layered structure of  $\text{CrX}_3$ , the  $\text{Cr}^{3+}$  cations within the layers adopt a honeycomb network of edge-sharing  $\text{CrX}_6$  octahedra character [5]. The  $\text{CrI}_3$  has the largest magnetic ordering temperature  $T_c$  of 68 K among the chromium trihalides, and the FM order is maintained even down to monolayer with temperature as high as 45 K [6,7]. In contrast to  $\text{CrX}_3$ , ternary compounds  $\text{Cr}_2\text{Z}_2\text{Te}_6$  ( $\text{Z} = \text{Si}$  and  $\text{Ge}$ ) possesses a similar layered crystal structure, with the centre of honeycomb network occupied by  $\text{Ge}_2$  dimers [8]. The Curie temperature  $T_c$  increases from 32 K for  $\text{Cr}_2\text{Si}_2\text{Te}_6$  to 66 K for  $\text{Cr}_2\text{Ge}_2\text{Te}_6$  [9-11]. As a Heisenberg's 2D ferromagnetic with strong magnetic anisotropy, the monolayer of  $\text{Cr}_2\text{Ge}_2\text{Te}_6$  is primarily single ion anisotropy, but its Curie temperature drops to 22 K [4].

Application of high pressure is an efficient route to regulate the electronic and magnetic properties of 2-D vdW compounds. For example, pressure has been successfully used to control the magnetism in both samples of a few atomic layers and bulk single crystals of  $\text{CrI}_3$  [12-14]. Cr-based vdW charge transfer insulators,  $\text{Cr}_2\text{X}_2\text{Te}_6$  ( $\text{X} = \text{Si}$  and  $\text{Ge}$ ) with ferromagnetic ground state are promising 2D materials for exploring the interplay between magnetic and electrical properties and have been subject of many recent studies. A recent study on the  $\text{Cr}_2\text{Si}_2\text{Te}_6$  demonstrated concurrent structural phase transition and insulator-metal transition followed by superconductivity at  $\sim 7.5$  GPa [15], while in  $\text{Cr}_2\text{Ge}_2\text{Te}_6$ , no superconductivity was observed at comparable pressure [16]. Recent studies reveal that the Curie temperature  $T_c$  of  $\text{Cr}_2\text{Ge}_2\text{Te}_6$  decreases by about 18% between 0-4.5 GPa, however upon further pressurisation the  $T_c$  start to increase and  $\text{Cr}_2\text{Ge}_2\text{Te}_6$  transforms from a ferromagnetic insulator to a correlated 2-D Fermi metal at 7.0 GPa with  $T_c$  exceeding  $\sim 250$  K at 9.1 GPa [17-19]. Understanding the origin of these drastic electronic effects, requires investigating the pressure effects on the crystal structures of  $\text{Cr}_2\text{Ge}_2\text{Te}_6$ . The phase stability

of  $\text{Cr}_2\text{Ge}_2\text{Te}_6$  has been studied using high pressure powder X-ray diffraction and Raman spectroscopy, but the observations were inconsistent when different pressure transmitting medium (PTM) were utilized [20-22]. These inconsistencies prompt us to investigate the structural stability and the onset metallization pressure of the  $\text{Cr}_2\text{Ge}_2\text{Te}_6$  under hydrostatic pressure.

In this work, we study the structural and electronic properties of  $\text{Cr}_2\text{Ge}_2\text{Te}_6$  single crystals using high pressure synchrotron single crystal X-ray diffraction and electrical resistance measurements in diamond anvil cells together with first-principles calculations. Using helium as the PTM in the X-ray measurements, we accurately determined the crystal structures of  $\text{Cr}_2\text{Ge}_2\text{Te}_6$  under high pressure and in contrast to previous studies we show that there is no phase transition below  $\sim 20.0$  GPa. Further compression leads to an irreversible amorphization in  $\text{Cr}_2\text{Ge}_2\text{Te}_6$ . Electrical transport measurements showed a complete insulator-metal transformation occurred at  $\sim 3.9$  GPa in  $\text{Cr}_2\text{Ge}_2\text{Te}_6$ , which is much lower than previously reported values of 7-14 GPa. DFT calculations reveal a distinct insulator to metal transition which takes place at 3.2 GPa consistent with our experiments and suggest that a large reduction of Cr-Te bond lengths within  $\text{CrTe}_6$  octahedra is most likely responsible for the band gap closure.

## II. EXPERIMENTAL AND THEORETICAL METHODS

**Synthesis of  $\text{Cr}_2\text{Ge}_2\text{Te}_6$  single crystals.** The  $\text{Cr}_2\text{Ge}_2\text{Te}_6$  single crystals are grown by the self-flux method [23]. The starting materials of 2 mmol of Cr (99.999%, Sigma Aldrich) and 2 mmol Ge (99.999%, Sigma Aldrich) powders were initially mixed with the molar ratio of 1:1, and an excess of 24 mmol of Te powder was used as the flux. The mixture was loaded and flame-sealed in a silica ampule under high vacuum pressure of  $10^{-5}$  Pa. The mixture was heated at 700 °C for two weeks and slowly cooled to 500 °C with a rate of 5°C/h and then excess Te was removed by the centrifugation process. Finally, plate-like single crystals with silvery lustre were obtained. The sample purity was confirmed both by single crystal and powder X-ray diffraction.

**High pressure X-ray diffraction measurements.** The Boehler-Almax plate diamond anvil cells (DACs) with 500  $\mu\text{m}$  culet size and a large opening angle of  $\sim 60^\circ$  were used in the high-pressure single-crystal X-ray measurements. Pressure was calibrated by the ruby

fluorescence method and was measured before and after each diffraction data collection [24].

Unlike the previous experiments, in which the 4:1 methanol-ethanol mixture [21] and silicone oil [22] were used as pressure-transmitting media, we chose the helium (He) as the pressure transmitting medium (PTM). Plate-shaped single crystal of  $\text{Cr}_2\text{Ge}_2\text{Te}_6$  with the dimension of  $\sim 28 \times 25 \times 10 \mu\text{m}^3$  was loaded in the  $\sim 220 \mu\text{m}$  diameter and  $\sim 65 \mu\text{m}$  thickness rhenium gasket chambers. The high-pressure single-crystal X-ray data were collected up to 19.5 GPa, above which only powder diffraction data were recorded at room temperature. For data above 20 GPa, only powder X-ray diffraction from the wide  $\phi$  angle scan was collected and cleaned XRD patterns data were obtained by removing the background (gasket and solid helium and diamond) [25].

All high-pressure single-crystal X-ray diffraction data of  $\text{Cr}_2\text{Ge}_2\text{Te}_6$  were collected at 13-BM-C beamline, GSECARS of the Advanced Photon Source (APS), Argonne National Laboratory (ANL) with X-ray wavelength of 0.4341 Å. Single crystal diffraction data were recorded using a PILATUS3 1M (Dectris) detector. The exposure time was set as 1s/degree, and each diffraction image covered 1 degree on the  $\phi$ -axis. The collected X-ray data were indexed and reduced using the APEX3 package. The crystal structures of  $\text{Cr}_2\text{Ge}_2\text{Te}_6$  can be solved by the direct method using SHELXS-97 [26] and refined with SHELXL interfaced by Olex2-1.5 [27]. All the Cr, Ge, and Te atoms were refined anisotropically. The selected crystallographic parameters and structure information were summarized in Supplemental Material Table S1 and Table S2, respectively [28].

In order to examine the phase stabilities of the ambient pressure structure and mimic identical hydrostatic conditions of electrical transport measurements, additional high pressure synchrotron powder X-ray measurements of  $\text{Cr}_2\text{Ge}_2\text{Te}_6$  were performed using NaCl as the PTM. The X-ray data at room temperature were collected at 16-ID-B, HPCAT, APS ( $\lambda = 0.4246$  Å). The diffraction images were integrated using the Dioptas 0.5.1 software [29], and X-ray data were fitted by Le Bail fitting method using GSAS-EXPGUI package [30] and the single crystal structures of  $\text{Cr}_2\text{Ge}_2\text{Te}_6$  were used as the starting models to carry out all the data refinements.

**High pressure electrical transport measurements of  $\text{Cr}_2\text{Ge}_2\text{Te}_6$  single crystal.** High pressure electrical resistance measurements of  $\text{Cr}_2\text{Ge}_2\text{Te}_6$  single crystal were conducted by

a four-terminal method. A fine mixture of alumina powder and epoxy was used to insulate the electrodes and gasket. A 500  $\mu\text{m}$  culet size DAC was used for all the measurements. Stainless steel gaskets with a  $\sim 300$   $\mu\text{m}$  hole filled with the alumina-epoxy mixture and compressed to  $\sim 7.0$  GPa and then released to ambient pressure. And a  $\sim 130$   $\mu\text{m}$  hole was laser-drilled in the compressed insulated gasket. Fine NaCl powder was inserted in the hole acting as the pressure medium and the powder was initially compressed to  $\sim 2.0$  GPa till it turned transparent. A plate-like  $\text{Cr}_2\text{Ge}_2\text{Te}_6$  single crystal was carefully loaded on the top of the compressed NaCl, and four platinum electrodes with the thickness of 5  $\mu\text{m}$  were arranged to contact the sample. The *dc* electrical resistivity of the sample was measured using a current of 50-200  $\mu\text{A}$ . A closed cycle helium cryostat was employed to examine the temperature dependence of the electrical resistance at specific pressures in the range of 2.4 to 300 K. Pressure was determined using the ruby fluorescence method both at room temperature and low temperature of  $\sim 4.0$  K with the aid of an online ruby system.

**Electronic Structure Calculations.** The electronic structures calculations of  $\text{Cr}_2\text{Ge}_2\text{Te}_6$  were performed using density functional theory (DFT) based on projector augmented wave (PAW) method, as implemented in the Vienna ab initio simulation package (VASP) [31]. The exchange-correlation interactions were depicted within the generalised gradient approximation (GGA) [32,33] as formulated by Perdew-Burke-Ernzerhof (PBE) [34]. The plane-wave cutoff energy of 450 eV and  $\Gamma$ -central  $9 \times 9 \times 3$  k-point mesh were adopted. The high-symmetry path used in band structure calculations is set along  $\Gamma$ -A-H-K- $\Gamma$ -M-L-H, and the high symmetry points  $\Gamma$ , A, H, K, M and L are (0, 0, 0), (0, 0, 0.5), (0.333, 0.667, 0.5), (0.333, 0.667, 0), (0, 0.5, 0) and (0, 0.5, 0.5), respectively. The Cr  $3d^54s^1$ , Ge  $4s^24p^2$ , and Te  $5s^25p^4$  electrons were treated explicitly in all calculations. Besides, the effective value of  $U = 1.0$  eV was utilized to treat the on-site Coulomb interaction of localized electrons [35]. Electron localization function (ELF) was calculated to describe and visualize chemical bonds in the  $\text{Cr}_2\text{Ge}_2\text{Te}_6$  structures at selective pressures [36]. To avoid the error induced from computational methods and match the experimental results, we performed DFT calculations using the experimental lattice parameters and only relaxed the atomic positions within lattices in all DFT calculations. The force per atom was set to be less than 0.01 eV/ $\text{\AA}$ .

### III. RESULTS AND DISCUSSION

## A. Structure evolution under pressure

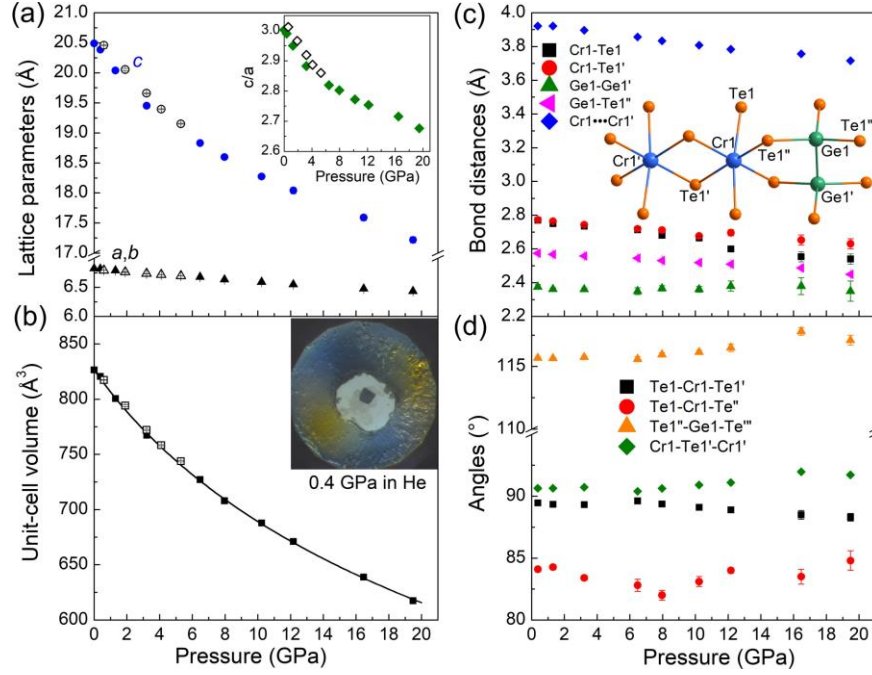


**Figure 1.** (a) Lattice parameters of  $\text{Cr}_2\text{Ge}_2\text{Te}_6$  as a function of pressure. The inset indicates the pressure dependence of  $c/a$  ratio. (b) The third-order Birch-Murnaghan equations of states (EoS) fit the unit-cell volume data. The inset displays a bulk single crystal of  $\text{Cr}_2\text{Ge}_2\text{Te}_6$  compressed in helium at 0.4 GPa. The powder X-ray data using NaCl as the PTM are indicated as unfilled symbols. (c) Changes in bond distances under compression. The coordination environments of Cr1 and Ge1 atoms are shown in the inset. (d) Evolution of Te-Cr-Te and Te-Ge-Te angles under pressure.

The crystal structures of  $\text{Cr}_2\text{Ge}_2\text{Te}_6$  under high pressure were determined by the synchrotron X-ray diffraction method at room temperature. Unlike the previous powder X-ray diffraction experiments, in which silicone oil or 4:1 methanol-ethanol mixture was employed as the pressure transmitting medium (PTM) [19,22]. In our work, we used helium (He) as the PTM for all the diffraction experiments, since helium was proved to be one of the best PTM and it could provide good hydrostaticity at least to 20 GPa [37]. As shown in Figure 1, we did not observe crystalline-crystalline structure phase transition through the whole range from ambient pressure to ~20 GPa. Above ~20 GPa, the  $\text{Cr}_2\text{Ge}_2\text{Te}_6$  sample starts undergoing crystalline-amorphous transition, which hampers the determination of the lattice parameters. With pressure increased to 31.2 GPa, the intensities of reflections (spots) from the sample are much weaker than that at 19.5 GPa and the diffraction peaks become wider (*e.g.* 8-10°). These indications reveal the sample gradually



amorphized under compression and it still maintains its crystallinity partially at 31.2 GPa. Hence the crystalline phase coexists with the amorphous state at 31.2 GPa. A complete amorphization could be expected to observe at even much higher pressures (see Supplemental Material Figure S1 [28]). In the previous reports using silicone oil/methanol-ethanol mixture as the pressure media, a new phase II was detected above 7.0/14.0/18.3 GPa [19,21,22], we attribute to the origin of these discrepancies to the presence of deviatoric stress which especially can be prominent in 2-D materials [38]. Interestingly, in our powder X-ray diffraction studies using NaCl as the PTM, no phase transition occurred up to 5.2 GPa at room temperature, well consistent with the previous reports (Figure S2). It is well-known that the XRD patterns are commonly broadened under non-/quasi-hydrostatic environments, these wide diffraction peaks may provide fake information for the identification of a new phase [39]. As shown in Figure 1a, the lattice parameters of  $\text{Cr}_2\text{Ge}_2\text{Te}_6$  shrink monotonically with increasing pressure, the  $c$  axis has the largest compressibility due to the compressible vdW interactions, while  $a$  and  $b$  axes are very rigid within the layers. For example, the  $c$  axis is reduced by  $\sim 16.0\%$  up to 19.5 GPa, where  $a$  and  $b$  axes decrease almost 3 times smaller: only compressed by  $\sim 5.7\%$ . It is obvious that the [001] is the soft direction, which is well consistent with the 2-D layered structure. As shown in Figure 1b, the unit-cell volume decreases gradually with increasing pressure, indicative of no phase transition occurring up to  $\sim 20$  GPa. The results indicate that the ambient-pressure phase of  $\text{Cr}_2\text{Ge}_2\text{Te}_6$  is robust against pressure before the amorphization. The volume data  $V(P)$  can be well fitted by the third-order Birch Murnaghan equation of state, the zero-pressure bulk modulus  $B_0$  is 39.2(13) GPa and its pressure derivative  $B'$  equals to 3.8(3). The magnitude of  $B_0$  is comparable to the analogous compound  $\text{Cr}_2\text{Si}_2\text{Te}_6$  (37(1) GPa) [40].

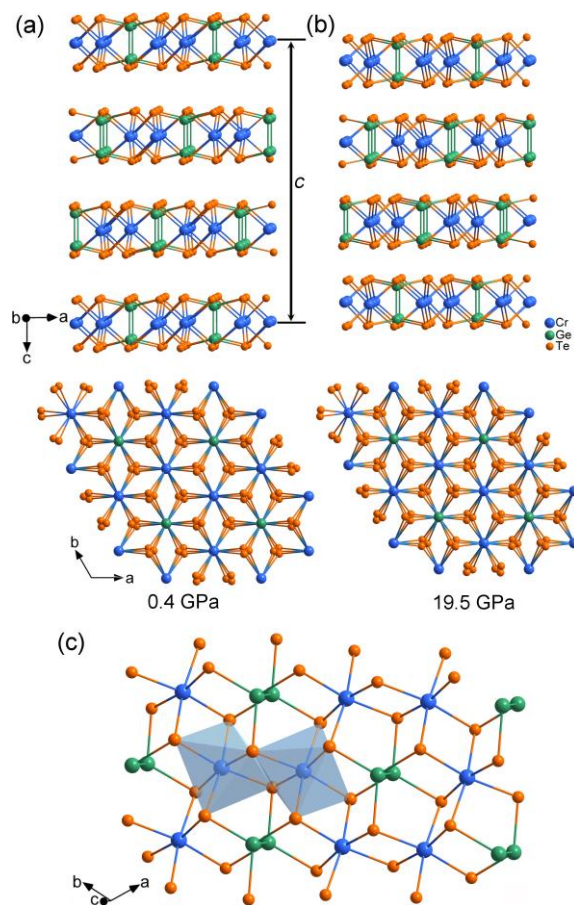


**Figure 2.** (a) Crystal structures of  $\text{Cr}_2\text{Ge}_2\text{Te}_6$  at 0.4 GPa viewed along the [010] and [001] directions. (b) Structures at 19.5 GPa viewed along the same directions as 0.4 GPa. (c) single layer of  $\text{Cr}_2\text{Ge}_2\text{Te}_6$  viewed approximately along the  $c$  axis. The edge-sharing  $\text{CrTe}_6$  octahedra are indicated.

At ambient conditions, the structure of  $\text{Cr}_2\text{Ge}_2\text{Te}_6$  adopts a typical lamellar structure type, with one Cr, one Ge and one Te atoms in the asymmetric unit [11,41]. The structure features a rhombohedral system with space group  $R\bar{3}$  and  $Z = 3$ . The edge-sharing  $\text{CrTe}_6$  octahedra form a honeycomb network with the rest free spaces of the centre occupied by  $\text{Ge}_2$  dimers and these layers are interacted with weak vdW interactions and packed along the  $c$  axis (Figure 2a). It can be easily seen that the structure of  $\text{Cr}_2\text{Ge}_2\text{Te}_6$  is derived from the known ferromagnetic insulator  $\text{CrI}_3$ , in which the positions of  $\text{Ge}_2$  dimers are absent [5]. The Cr1 atom adopts an octahedral geometry and is coordinated to six Te1 atoms and these octahedra are interconnected via an edge-sharing manner (Figure 2c). From the single crystal X-ray data refinements, the atomic coordinates of Cr, Ge and Te under high pressure are accurately determined, which allow us to analyse the detailed structural evolution under

compression. The Cr1–Te1 bond distance shrinks from 2.769(7) Å at 0.4 GPa to 2.54(3) Å at 19.5 GPa, while the Te1–Cr1–Te1' angle decreases slightly from 89.46(7)° to 88.3(3)°. The Cr1···Cr1' distances are shortened from 3.9216(3) to 3.7157(15) Å when pressure increases from 0.4 to 19.5 GPa and the Cr1–Te'–Cr1' angle changes slightly from 90.65(5)° to 91.73(11)° (Figure 1c). The Te<sub>3</sub>–Ge1–Ge1–Te<sub>3</sub> unit which is parallel to the *c* axis undergoes slight distortions under compression. For example, the Ge1–Te1'' bond distance decreases from 2.574(2) Å at 0.4 GPa to 2.449(7) Å at 19.5 GPa, while the Ge1–Ge1' bond lengths are hard to compress, *i.e.* 2.375(13) Å (at 0.4 GPa) *vs.* 2.35(6) Å (at 19.5 GPa).

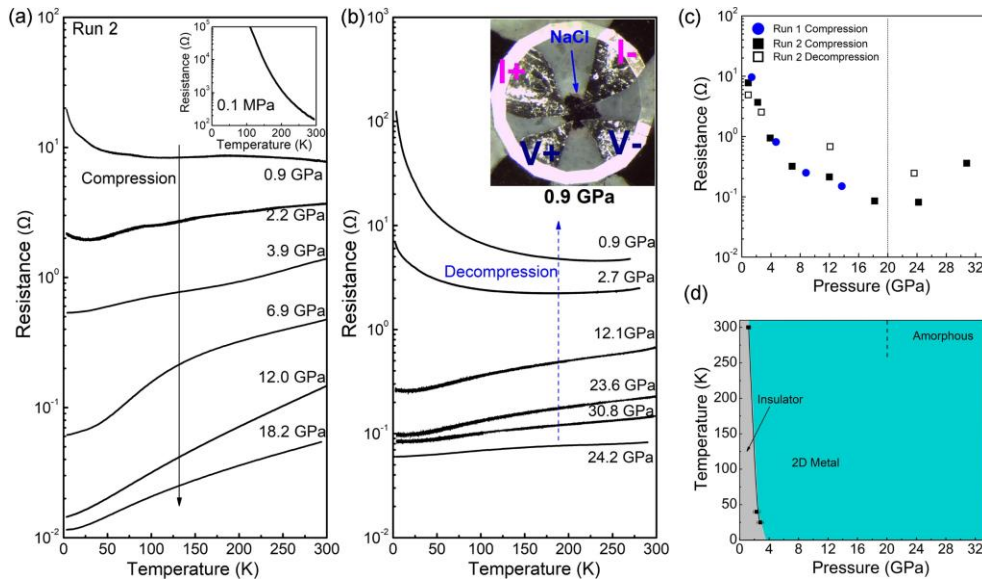


**Figure 3.** (a) Electrical resistance of Cr<sub>2</sub>Ge<sub>2</sub>Te<sub>6</sub> in the crystalline phase range (below 20 GPa). The inset indicates the data measured in a different single crystal at ambient pressure. (b) Electrical resistance data in the amorphous phase above 20 GPa. The inset shows the photograph of Cr<sub>2</sub>Ge<sub>2</sub>Te<sub>6</sub> single crystal immersed in the NaCl medium at 0.9 GPa using the four-terminal method for the measurements. (c) Pressure-dependent electrical resistances of Cr<sub>2</sub>Ge<sub>2</sub>Te<sub>6</sub> at room temperature. (d) *P*-*T* phase diagram Cr<sub>2</sub>Ge<sub>2</sub>Te<sub>6</sub> based on the X-ray and electrical resistance data.

## B. Pressure-induced insulator-to-metal transition

We also performed electrical transport properties of Cr<sub>2</sub>Ge<sub>2</sub>Te<sub>6</sub> under high pressure on a single crystal sample with NaCl as the PTM. As shown in Figure 3a, the electrical resistance decreases monotonically under compression in the range of crystalline phase  $R\bar{3}$ . The single crystal sample shows a distinct insulator behaviour at ambient pressure, its resistance increases rapidly upon cooling. To confirm the onset of the metallization

pressure, we measured the temperature dependence of electrical resistance under variable pressures. As shown in Figure 3a and 3b, the  $R(T)$  curve shows negative  $dR/dT$  at 0.9 GPa, indicative of semiconductor character. At 2.2 GPa, the  $dR/dT$  demonstrates positive in the high temperature region, whereas it changes to negative in low temperature region, *e.g.* 40 K at 2.3 GPa. With increasing the pressure to 3.9 GPa, the  $dR/dT > 0$  through the whole temperature range of 2.4-300 K, and together with structural data this implies that the sample becomes a 2-D metal (Supplemental Material, Figure S2 [28]). The onset of metallization pressure observed here is much lower than the recent report of 7.0 GPa (close to the solidification pressure of the PTM), in which the resistivity measurements were performed in a cubic anvil cell with 1:1 ratio of Flourinert FC70 and FC77 as the PTM [16]. The mixture of FC70 and FC77 has hydrostatic limit of  $\sim 1.0$  GPa, hence quasi-hydrostatic environments will be appeared in the range of 1.0 and 7.0 GPa [42,43]. As discussed above, our powder X-ray diffraction measurements using NaCl as the PTM confirm that no phase transition took place up to 5.2 GPa, hence the semiconductor-to-metal transition of  $\text{Cr}_2\text{Ge}_2\text{Te}_6$  is not related to the phase transformation, but its intrinsic electronic changes. At 3.9 GPa,  $R(T)$  follows a power law  $R(T) = R_0 + AT^n$  below 30 K, with an exponent  $n \sim 1.95$ , an indication of Fermi liquid state (Supplemental Material, Figure S4 [28]). Unlike the previous resistivity measurements within the *ab* plane of  $\text{Cr}_2\text{Ge}_2\text{Te}_6$  single crystal, we did not observe obvious anomaly in electrical resistivity data, which hinders us to trace the evolution of the Curie temperature under compression [16]. Interestingly, with further increasing the pressure above 3.9 GPa, we did not observe the superconductivity down to 2.4 K prior to the crystalline-amorphous transformation occurs, while in the analogous material  $\text{Cr}_2\text{Si}_2\text{Te}_6$ , superconductivity emerges at  $\sim 7.5$  GPa [15]. After pressure releasing from the maximum pressure of 30.8 GPa to 0.9 GPa, we found the  $R(T)$  curves are irreversible compared to the initial compression data (*e.g.* at 0.9 GPa), revealing the crystalline-amorphous transformation could not be recovered; well consistent with the X-ray diffraction data. Like the previous observations [22], the electrical resistance decreases gradually under compression in the crystalline phase, and it goes up after the amorphization occurred above 20 GPa (see Figure 3c). We constructed the  $P$ - $T$  phase diagram from the X-ray and electrical resistance data, it can be clearly seen that the

metallization pressure increases gradually upon cooling, and the sample undergoes a complete insulator-metal transition around 4.0 GPa below 10 K (see Figure 3d).

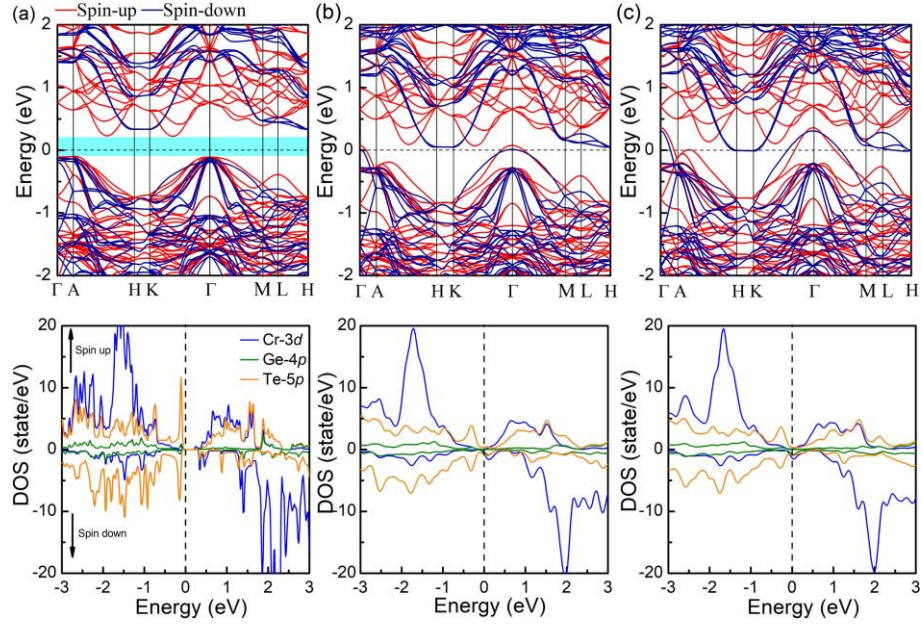


**Figure 4.** Calculated electronic band structures and density of states at (a) 0.4 GPa, (b) 3.2 GPa and (c) 6.5 GPa.

### C. DFT calculations

To gain insights into the chemical bonding of  $\text{Cr}_2\text{Ge}_2\text{Te}_6$ , we calculated the electron localization function (ELF) at selective pressures (Supplemental Material, Figure S5). The large difference in ELF between Cr and Te atoms indicates the ionic bonding characteristics, where the charge transfers are from less electronegative Cr to more electronegative Te. There exists a charge localization between Ge-Ge bonds, demonstrating the covalent bonding feature. As shown in Table S3, we found through Bader charge analysis the charges on the Cr atom at 0.4 and 19.5 GPa are largely decreased ( $0.86e$  vs  $0.68e$ ), revealing that the charge transfer from Cr to Te reduces under compression, whereas the charge on the Ge atom is slightly decreased ( $0.28e$  vs  $0.21e$ ).

To better understand the electronic structure evolution of  $\text{Cr}_2\text{Ge}_2\text{Te}_6$  under pressure, we performed DFT calculations based on the relaxed structures of experimental single crystal X-ray data. The calculated band structures of  $\text{Cr}_2\text{Ge}_2\text{Te}_6$  at 0.4 GPa indicate that band gap is indirect, with the valence band maximum located at A point and the conduction band minimum settled between K and  $\Gamma$  points (Figure 4a). The calculated band gap is 0.32 eV

at 0.4 GPa, and it decreases to 0.2 eV when the pressure increases to 1.3 GPa. At 3.2 GPa, we observed obvious band gap closure when the valence bands cross the Fermi level (Supplemental Material, Figure S6 [28]). The insulator-to-metal transition is most likely correlated to the large shrinkage of the Cr-Te bond lengths upon compression (Figure 1c). The metallization pressure observed here is in good agreement with our electrical transport measurements, but much lower than the previous reports of 7-14 GPa [19,22]. It is notable that in a recent work where GGA method is used to determine the band gaps of  $\text{Cr}_2\text{Ge}_2\text{Te}_6$ , insulator to metal transition is calculated to occur at 6.0 GPa, which is well consistent with the powder X-ray diffraction measurements performed in the same study under non-hydrostatic conditions ( $c/a$  ratio displays prominent kink around 7.5 GPa, indicative of isosymmetric transformation) [19]. In our case, where the  $\text{Cr}_2\text{Ge}_2\text{Te}_6$  sample was studied under hydrostatic conditions, and it does not undergo phase transition up to 20 GPa, hence the band gap closure is primarily arising from large reductions of bond lengths. To understand the contributions of Cr, Ge, and Te orbital states, we plotted the density of states (DOS) as a function of pressure. Here we compare the partial density of states in three selected pressures of 0.4 GPa, 3.2 GPa, and 6.5 GPa. At 0.4 GPa, both conduction and valence density of states are mainly occupied by the Cr-3*d* and Te-5*p* states, while the Ge-4*p* states play a minor role in the contributions of the total density of states. The observed *p-d* band gap demonstrates a charge transfer insulator character (Figure 4a) [44]. At 3.2 GPa, Cr-3*d* and Te-5*p* states cross the Fermi level, indicating metallic character. Unlike the 2-D VdW phosphorus trichalcogenides  $\text{MnPS}_3$ , in which the insulator to metal transformation generally correlates to the spin state transition and structural transformation with large volume collapse [45]. Moreover, the isostructural compound  $\text{Cr}_2\text{Si}_2\text{Te}_6$  exhibits a concurrent insulator-metal transition and structural transition and superconductivity at  $\sim 7.5$  GPa [15]. However, in  $\text{Cr}_2\text{Ge}_2\text{Te}_6$ , the absence of structural transition in the insulator to metal transformation implies that pressure modified electronic ground states is purely electronic and the large contraction of Cr-Te bond distances are most likely responsible for the metallization [16].

#### IV. CONCLUSIONS

In summary, the crystallographic and electrical transport properties of 2-D  $\text{Cr}_2\text{Ge}_2\text{Te}_6$  single crystal have been investigated by combinations of experimental and DFT calculations. Our high-pressure single crystal X-ray diffraction measurements using helium as the PTM reveal that the ambient-pressure rhombohedral structure of  $\text{Cr}_2\text{Ge}_2\text{Te}_6$  is very robust. The interlayer distances show the largest compressibility along the  $c$  axis and there is no phase transition that takes place up to  $\sim 20$  GPa. Above 20 GPa, the  $\text{Cr}_2\text{Ge}_2\text{Te}_6$  sample starts to lose its crystallinity and the crystalline phase and amorphous state coexist even at the maximum pressure of 31.2 GPa. A prominent insulator-to-metal transition takes place at 3.9 GPa from the electrical transport measurements on the  $\text{Cr}_2\text{Ge}_2\text{Te}_6$  single crystal with NaCl is used as the PTM, well consistent with the DFT calculations. The observed onset of metallization pressure of  $\text{Cr}_2\text{Ge}_2\text{Te}_6$  takes place at considerably lower than previous reports of 7-14 GPa. Our powder X-ray diffraction measurements using NaCl as the PTM reveal the absence of the phase transition of  $\text{Cr}_2\text{Ge}_2\text{Te}_6$  at 3.9 GPa, hence the metallization of the sample is intrinsically from its electronic changes under compression. The distinct band gap closure demonstrates compression-induced electronic changes in this 2-D material as a consequence of the contraction of Cr-Te bonds lengths. Unlike the isostructural  $\text{Cr}_2\text{Si}_2\text{Te}_6$ , we did not observe superconductivity down to 2.4 K in the whole crystalline phase region. This study sheds light on the interplay between crystal structure and electronic properties of layered 2-D materials and demonstrates the phase stability and metallization in this system may be strongly related to the different hydrostatic environments.

## ACKNOWLEDGMENTS

W. C. would like to acknowledge the startup funding provided by University of Electronic Science and Technology of China (A1098531023601326). We thank Dr. Jiangang He for fruitful discussions. We thank A. Dockery, A. Glende, F. Safari, M. Burden, I. Saffarian-Deemyad, J. St. Andre and T. McNamee and for help with high pressure X-Ray data collection. The authors would like to acknowledge S. Tkachev for the assistance of helium gas loading for the single crystal X-ray measurements and J. Smith and C. Kenney-Benson for providing experimental support at HPCAT. The high-pressure single crystal X-ray diffraction data and powder X-ray diffraction data were collected at 13-BM-C of

GeoSoilEnviroCARS (The University of Chicago, Sector 13) and at 16-ID-B of HPCAT (Sector 16), Advanced Photon Source (APS), Argonne National Laboratory, respectively. GeoSoilEnviroCARS is supported by the National Science Foundation-Earth Sciences (EAR-1634415) and Department of Energy-GeoSciences (DE-FG02-94ER14466). HPCAT operations are supported by DOE-NNSA's Office of Experimental Sciences. Use of the COMPRES-GSECARS gas loading system and PX2 was supported by COMPRES under NSF Cooperative Agreement EAR-1661511 and by GSECARS through NSF grant EAR-1634415 and DOE grant DE-FG02-94ER14466. Work at Argonne (sample preparation, characterization and crystal growth) is supported by the U.S. DOE, Office of Basic Energy Science, Materials Science and Engineering Division. Use of the Advanced Photon Source at Argonne National Laboratory was supported by the U.S. Department of Energy, Office of Science, Office of Basic Energy Sciences, under Contract No. DE-AC02-06CH11357.

## REFERENCES

- [1] K. S. Burch, D. Mandrus, and J.-G. Park, *Nature* **563**, 47 (2018).
- [2] C. Felser, G. H. Fecher, and B. Balke, *Angew. Chem. Int. Ed.* **46**, 668 (2007).
- [3] B. Huang, G. Clark, D. R. Klein, D. MacNeill, E. Navarro-Moratalla, K. L. Seyler, N. Wilson, M. A. McGuire, D. H. Cobden, D. Xiao *et al.*, *Nat. Nanotechnol.* **13**, 544 (2018).
- [4] C. Gong, L. Li, Z. Li, H. Ji, A. Stern, Y. Xia, T. Cao, W. Bao, C. Wang, Y. Wang *et al.*, *Nature* **546**, 265 (2017).
- [5] M. A. McGuire, H. Dixit, V. R. Cooper, and B. C. Sales, *Chem. Mater.* **27**, 612 (2015).
- [6] B. Huang, G. Clark, E. Navarro-Moratalla, D. R. Klein, R. Cheng, K. L. Seyler, D. Zhong, E. Schmidgall, M. A. McGuire, D. H. Cobden *et al.*, *Nature* **546**, 270 (2017).
- [7] J. F. Dillon and C. E. Olson, *J. Appl. Phys.* **36**, 1259 (1965).
- [8] B. Siberchicot, S. Jobic, V. Carteaux, P. Gressier, and G. Ouvrard, *J. Phys. Chem.* **100**, 5863 (1996).
- [9] V. Carteaux, F. Moussa, and M. Spiesser, *Europhys. Lett.* **29**, 251 (1995).
- [10] G. Ouvrard, E. Sandre, and R. Brec, *J. Solid State Chem.* **73**, 27 (1988).
- [11] V. Carteaux, D. Brunet, G. Ouvrard, and G. Andre, *J. Phys. Condens. Matter.* **7**, 69 (1995).
- [12] T. Li, S. Jiang, N. Sivadas, Z. Wang, Y. Xu, D. Weber, J. E. Goldberger, K. Watanabe, T. Taniguchi, C. J. Fennie *et al.*, *Nat. Mater.* **18**, 1303 (2019).
- [13] T. Song, Z. Fei, M. Yankowitz, Z. Lin, Q. Jiang, K. Hwangbo, Q. Zhang, B. Sun, T. Taniguchi, K. Watanabe *et al.*, *Nat. Mater.* **18**, 1298 (2019).
- [14] S. Mondal, M. Kannan, M. Das, L. Govindaraj, R. Singha, B. Satpati, S. Arumugam, and P. Mandal, *Phys. Rev. B* **99**, 180407 (2019).
- [15] W. Cai, H. Sun, W. Xia, C. Wu, Y. Liu, H. Liu, Y. Gong, D.-X. Yao, Y. Guo, and M. Wang, *Phys. Rev. B* **102**, 144525 (2020).
- [16] D. Bhoi, J. Gouchi, N. Hiraoka, Y. Zhang, N. Ogita, T. Hasegawa, K. Kitagawa, H. Takagi, K. H. Kim, and Y. Uwatoko, *Phys. Rev. Lett.* **127**, 217203 (2021).
- [17] Y. Sun, R. C. Xiao, G. T. Lin, R. R. Zhang, L. S. Ling, Z. W. Ma, X. Luo, W. J. Lu, Y. P. Sun, and Z. G. Sheng, *Appl. Phys. Lett.* **112**, 072409 (2018).



- [18] Z. Lin, M. Lohmann, Z. A. Ali, C. Tang, J. Li, W. Xing, J. Zhong, S. Jia, W. Han, S. Coh *et al.*, Phys. Rev. Mater. **2**, 051004 (2018).
- [19] A. O. Fumega, S. Blanco-Canosa, H. Babu-Vasili, P. Gargiani, H. Li, J.-S. Zhou, F. Rivadulla, and V. Pardo, J. Mater. Chem. C **8**, 13582 (2020).
- [20] W. Ge, K. Xu, W. Xia, Z. Yu, H. Wang, X. Liu, J. Zhao, X. Wang, N. Yu, Z. Zou *et al.*, J. Alloys Compd. **819**, 153368 (2020).
- [21] E. Dong, B. Liu, Q. Dong, X. Shi, X. Ma, R. Liu, X. Zhu, X. Luo, X. Li, Y. Li *et al.*, Phys. B: Condens. Matter **595**, 412344 (2020).
- [22] Z. Yu, W. Xia, K. Xu, M. Xu, H. Wang, X. Wang, N. Yu, Z. Zou, J. Zhao, L. Wang *et al.*, J. Phys. Chem. C **123**, 13885 (2019).
- [23] H. Ji, R. A. Stokes, L. D. Alegria, E. C. Blomberg, M. A. Tanatar, A. Reijnders, L. M. Schoop, T. Liang, R. Prozorov, K. S. Burch *et al.*, J. Appl. Phys. **114**, 114907 (2013).
- [24] H. K. Mao, R. J. Hemley, Y. Wu, A. P. Jephcoat, L. W. Finger, C. S. Zha, and W. A. Bassett, Phys. Rev. Lett. **60**, 2649 (1988).
- [25] W. Cai, M. T. Hossain, J. Coles, J. Lybarger, J. Blanton, E. Sterer, and S. Deemyad, High Press. Res. **39**, 628 (2019).
- [26] G. Sheldrick, Acta Crystallogr. Sect. A Found. Crystallogr. **64**, 112 (2008).
- [27] O. V. Dolomanov, L. J. Bourhis, R. J. Gildea, J. A. K. Howard, and H. Puschmann, J. Appl. Crystallogr. **42**, 339 (2009).
- [28] See Supplemental Material at XXX for detailed structure information and electrical transport measurements data at various pressures.
- [29] C. Prescher and V. B. Prakapenka, High. Press. Res. **35**, 223 (2015).
- [30] B. Toby, J. Appl. Cryst. **34**, 210 (2001).
- [31] G. Kresse and J. Furthmüller, Phys. Rev. B **54**, 11169 (1996).
- [32] P. E. Blöchl, Phys. Rev. B **50**, 17953 (1994).
- [33] P. E. Blöchl, O. Jepsen, and O. K. Andersen, Phys. Rev. B **49**, 16223 (1994).
- [34] J. P. Perdew, K. Burke, and M. Ernzerhof, Phys. Rev. Lett. **77**, 3865 (1996).
- [35] Y. Fang, S. Wu, Z.-Z. Zhu, and G.-Y. Guo, Phys. Rev. B **98**, 125416 (2018).
- [36] A. D. Becke and K. E. Edgecombe, J. Chem. Phys. **92**, 5397 (1990).
- [37] S. Klotz, J. C. Chervin, P. Munsch, and G. L. Marchand, J. Phys. D: Appl. Phys. **42**, 075413 (2009).
- [38] L. Zhang, Y. Tang, A. R. Khan, M. M. Hasan, P. Wang, H. Yan, T. Yildirim, J. F. Torres, G. P. Neupane, Y. Zhang *et al.*, Adv. Sci. **7**, 2002697 (2020).
- [39] W. Cai, J. He, H. Li, R. Zhang, D. Zhang, D. Y. Chung, T. Bhowmick, C. Wolverton, M. G. Kanatzidis, and S. Deemyad, Nat. Commun. **12**, 1509 (2021).
- [40] K. Xu, Z. Yu, W. Xia, M. Xu, X. Mai, L. Wang, Y. Guo, X. Miao, and M. Xu, J. Phys. Chem. C **124**, 15600 (2020).
- [41] Y. Liu and C. Petrovic, Phys. Rev. B **96**, 054406 (2017).
- [42] T. Varga, A. P. Wilkinson, and R. J. Angel, Rev. Sci. Instrum. **74**, 4564 (2003).
- [43] V. A. Sidorov and R. A. Sadykov, J. Condens. Matter Phys. **17**, S3005 (2005).
- [44] P. Kuiper, G. Kruizinga, J. Ghijsen, G. A. Sawatzky, and H. Verweij, Phys. Rev. Lett. **62**, 221 (1989).
- [45] H.-S. Kim, K. Haule, and D. Vanderbilt, Phys. Rev. Lett. **123**, 236401 (2019).